Available online at www.sciencedirect.com
SCIENCE DIRECT®
Wear 259 (2005) 383–390
WEAR
www.elsevier.com/locate/wear

Corrosion and corrosive wear of annealed, impact-fractured and slow bending-fractured surface layers of AISI 1045 steel in a 3.5% NaCl solution

S.B. Yin *, D.Y. Li

Department of Chemical and Materials Engineering, University of Alberta, Edmonton, AB, Canada T6G 2G6

Received 31 July 2004; received in revised form 18 January 2005; accepted 1 February 2005
Available online 10 May 2005

Abstract

Previous studies have demonstrated that the wear-corrosion synergism can be markedly affected by the loading speed. In this study, effects of the loading speed or strain rate on corrosion and corrosive wear of annealed, impact-fractured and slow bending-fractured surface layers of AISI 1045 steel in a 3.5% NaCl solution were investigated using electrochemical, scanning Kelvin probing and electrochemical scratching techniques. In order to understand the mechanism responsible for the effects of loading speed on corrosion and corrosive wear, SEM fractography, X-ray line profile analysis and micro-hardness testing were employed to investigate changes in microstructure and corresponding mechanical properties with respect to the loading speed. Results of the experiments are explained in terms of the effect of strain rate on surface microstructure and corresponding electrochemical and mechanical properties, and consequently the corrosive wear behaviour of the steel.

Keywords: Corrosive wear; Strain rate; Microstructure; Defects

1. Introduction

In recent years, the synergism of wear and corrosion has become an important research area and attracted increasing interests [1]. The synergistic attack of wear and corrosion to metals is not well understood, since it involves several processes simultaneously, such as the formation and failure of passive films or adsorption layers, stress-accelerated corrosion and corrosion-accelerated wear, etc.

Since wear is a dynamic destructive process, the loading speed should also have a marked influence on wear. In many cases, the loading speed could be very high, for example, in the erosion-corrosion situation, the impact velocity of solid particles may reach 1000 m/s. In sliding wear processes, the sliding speed also varies significantly. It has been shown that the loading speed can considerably influence the wear-corrosion synergism [2,3] since mechanical properties, corrosion resistance and corresponding failure mode of a surface layer could be affected by the strain rate.

In order to predict corrosive wear under impact or a high-speed loading condition, one needs (1) to understand variations in surface microstructure and defect configuration arising from the dynamic loading and (2) to determine how electrochemical and mechanical properties change as a result of the microstructural variation. In addition, the dynamic aspect of wear-corrosion synergism also needs to be taken into account, which is, however, relatively difficult to deal with.

In the present study, effects of loading rate on the surface microstructure, defect configuration and consequent changes in mechanical properties, corrosion and corrosive wear behaviour of AISI 1045 steel were investigated. A 3.5% NaCl solution was chosen as the corrosive medium because of its relatively mild corrosivity with which the thin deformed surface layer (2–4 mm) would not be dissolved too quickly during the electrochemical and corrosive wear tests.

* Corresponding author. Tel.: +1 7804926607; fax: +1 7804922881.
E-mail address: syin@ualberta.ca (S.B. Yin).

0043-1648/$ – see front matter © 2005 Elsevier B.V. All rights reserved.
doi:10.1016/j.wear.2005.02.042

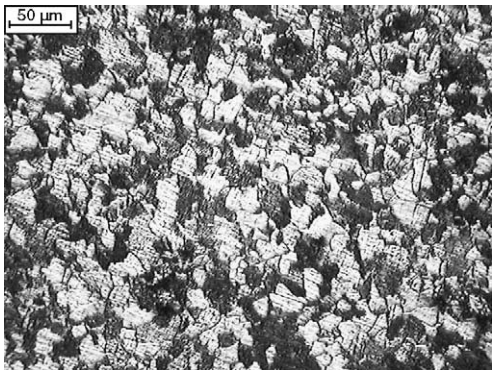

Fig. 1. Optical microstructure of the full-annealed 1045 steel.

2. Experimental

AISI 1045 steel (0.43–0.50 wt% C, 0.60–0.90 wt% Mn, maximum 0.04 wt% P, maximum 0.05 wt% S) was selected as a sample material. All samples were austenized at 810 °C for 45 min and quickly cooled down to and maintained at 640 °C for 30 min, followed by furnace cooling to room temperature. The microstructure of the sample was characterized by standard optical metallography (etchant: 2% NYTOL). Fig. 1 shows the optical microstructure of the steel sample, which is a typical hypo-eutectoid structure: Ferrite + Pearlite.

Samples for Charpy impact test were machined following the requirement specified in ASTM E 23 (Type A). The Charpy impact tests were performed at room temperature using a standard Charpy pendulum machine with a capacity of 360 J. Some of the Charpy samples were tested using a three-point-bending fixture in an Instron testing machine at a loading rate of 0.5 mm/min. Charpy absorbed energy (CVN) and the slow-bending absorbed energy were determined. Fracture surfaces generated by both the tests were examined using SEM.

Micro-hardness of the fractured surface layer was evaluated using a Fischerscope H100C micro-mechanical probe (Fisher Technology Ltd., Winsor, CT, USA). A standard Vickers diamond indenter was employed, which was pyramid-shaped and had an angle of 136° between faces. The indenter tip penetrated into the sample at a normal load that was increased continuously up to a designated level. The load was then gradually decreased back to zero. The entire loading and unloading processes were recorded automatically, resulting in a load-displacement curve. Hardness and elastic modulus could be determined from the curve, based on the attained stiffness of contact, contact depth and projected contact area. This system also incorporated a positioning device consisting of a microscope and a measuring stage, which allow precise location of the measurement point.

In order to qualitatively investigate the lattice distortions caused by deformation at different loading rates, residual microstrains in the fractured surface layers were determined through X-ray diffraction line profile analysis based on approximated profile shape-functions [4]. X-ray diffractograms of annealed, impact-fractured and slow bending-fractured surface layers were obtained using a Rigaku 3014 X-ray diffractometer with Cu Kα radiation, operated at 40 kV and 35 mA in a continuous-scan mode. The scanning speed was 0.2°/min. A graphite crystal monochromator was used to obtain monochromatization. Kα1 lines were separated from the combined Kα1 and Kα2 lines using a computer program. The full-annealed sample was used as a reference sample. (1 1 0) and (2 2 0) peaks were selected for the line profile analysis.

Electrochemical tests, including potentiodynamic polarization, linear polarization and Tafel plot measurements, were performed using a computerized Gamry PC4/750 electrochemical system. For all the electrochemical experiments, a saturated calomel electrode (SCE) and a platinum (Pt) net were used as the reference electrode and the counter electrode, respectively. The electrolyte solution was 3.5% NaCl. All the experiments were performed at room temperature (∼22 °C). The Potentiodynamic polarization experiments were performed at a scan rate of 0.33 mV/s.

At least three linear polarization corrosion tests were performed for each sample to measure its polarization resistance R_p, starting from 9.0 mV below the open circuit potential (OCP) and ending at 9.0 mV above OCP. The scanning rate was 0.05 mV/s.

At least three Tafel plot corrosion tests were performed for each sample, starting from 100 mV below OCP and ending at 140 mV above OCP. The scanning rate was 0.1 mV/s. The corrosion current density i_{corr} was calculated based on the following equation (ASTM standard G3-89):

$$i_{corr} = \frac{b_a b_c}{2.303(b_a + b_c)R_p}$$

where i_{corr} is the corrosion current density; b_a, the anodic Tafel slope; b_c, the cathodic Tafel slope; R_p, the linear polarization resistance.

A scanning Kelvin probe (SKP), provided by the KP Technology Ltd. (Caithness, UK), was employed to investigate the influence of strain rate on the surface electron work function (EWF). The KP system had three sub-systems, including a digital oscillator, data acquisition, and sample translation, which are controlled by a host PC. A three-axis microstepper positioner permitted high-resolution sample positioning (0.4 μm per step) and the scanning area was 2 mm × 2 mm. A gold tip with diameter equal to 1 mm was used. The oscillation frequency of the Kelvin probe was 173 Hz. Details of the system and the Kelvin method have been described in [5]. Before the KP test, the annealed samples were polished up to 600 grit abrasive papers and finally finished with 0.05 μm alumina. The impact-fractured samples and slow bending-fractured samples were tested with the original fracture surfaces.

Performances of the annealed, impact-fractured and slow bending-fractured surface layer during corrosive wear were evaluated using an electrochemical scratch technique, details

of which have been described in [6]. In this study, the corrosive medium was a 3.5% NaCl solution ($NaCl + H_2O$). The scratching tests were all performed under the open circuit potential. Surfaces of all the samples were polished using 600 grit abrasive paper and finally finished with 0.05 μm alumina. It should be indicated that the polishing treatment was carefully done to ensure that only a very thin surface layer of about 100–200 μm was removed, which should not affect the evaluation of surface layer's electrochemical properties and its resistance to corrosive wear, since the fractured surface layers were fairly thick (more than 2000 μm, estimated from microindentation tests). Three normal loads were used: 5 g, 10 g, 30 g. The moving speed of the tip was 6 mm/s. Sliding distance was 4 mm. The cross-sectional profiles of the scratch grooves were measured using an atomic force microscope (Digital Instrument, Santa Barbara, CA, USA). For each sample, three scratch tests were made and 12 or more cross-sectional profiles were measured. The wear loss was obtained by averaging 12 measurements, represented by the volume loss per unit length of the scratch groove (mm^3/mm).

3. Results and discussion

3.1. Surface microstructure and mechanical behaviour

Fig. 2 illustrates fracture surfaces caused by Charpy impact and slow-bending, respectively. The fractographs of the surface resulting from the Charpy impact test shows relatively brittle features, i.e. cleavage facet and river pattern (Fig. 2(a) and (b)), while the fracture surface of the slow-bending samples exhibits ductile features, i.e. micro-void coalescence (Fig. 2(c) and (d)). Microcracks were observed in surface layers (Fig. 3), which existed beneath the fracture surface of both types.

Absorbed energies of both the Charpy impact and slow-bending samples were measured and are illustrated in Fig. 4. As shown, the absorbed energy of the former is 32.5 J while that of the latter is 48.6 J. This absorption energy measurement is consistent with results of the SEM fractography examination, in which the impact fracture surface is relatively brittle and therefore consumed less energy during the fracture process.

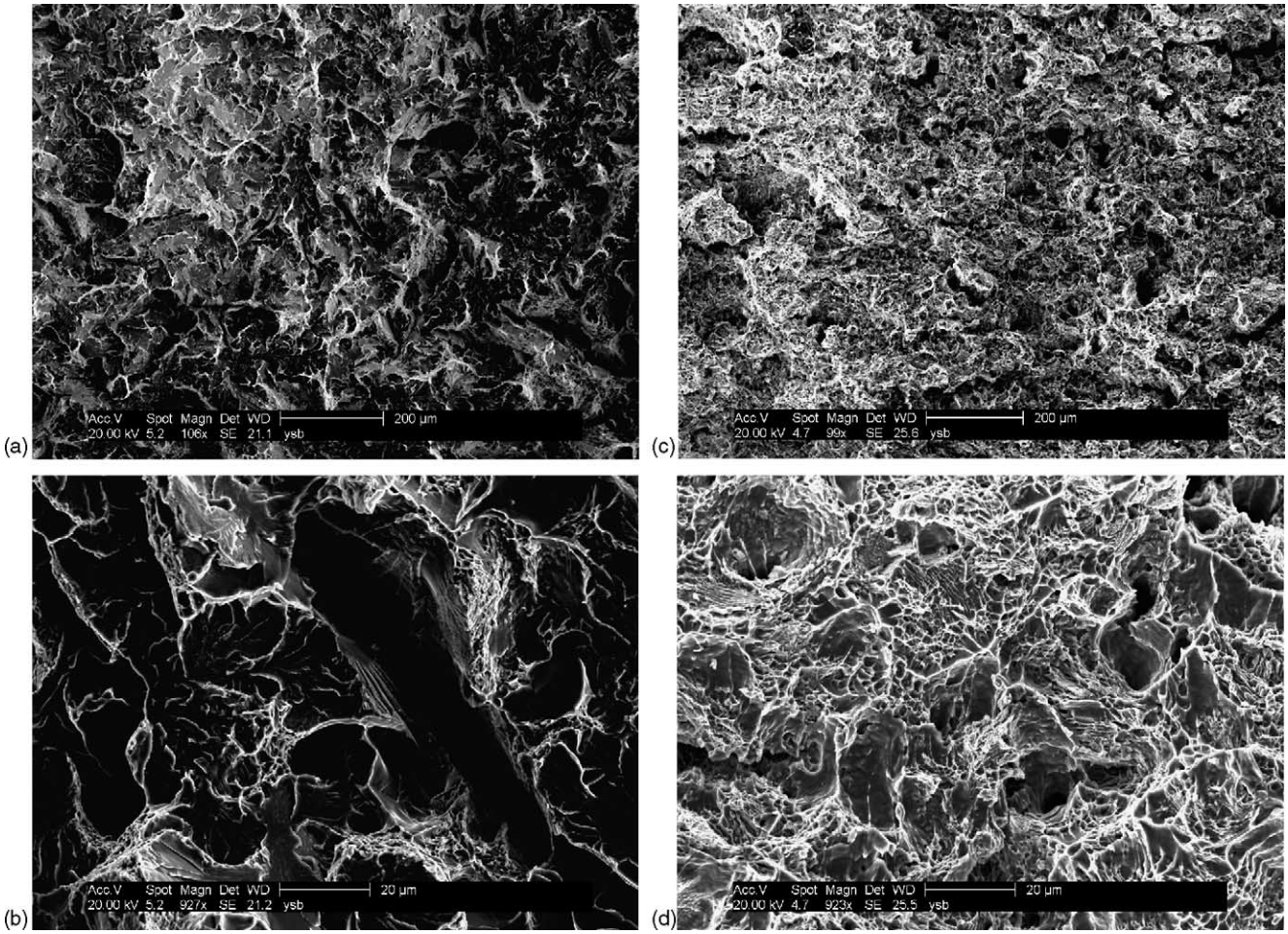

Fig. 2. SEM fracture surface morphology: (a) charpy impact fracture surface; (b) a closer view of the Charpy impact fracture surface; (c) slow bending fracture surface; (d) a closer view of the slow bending fracture surface.

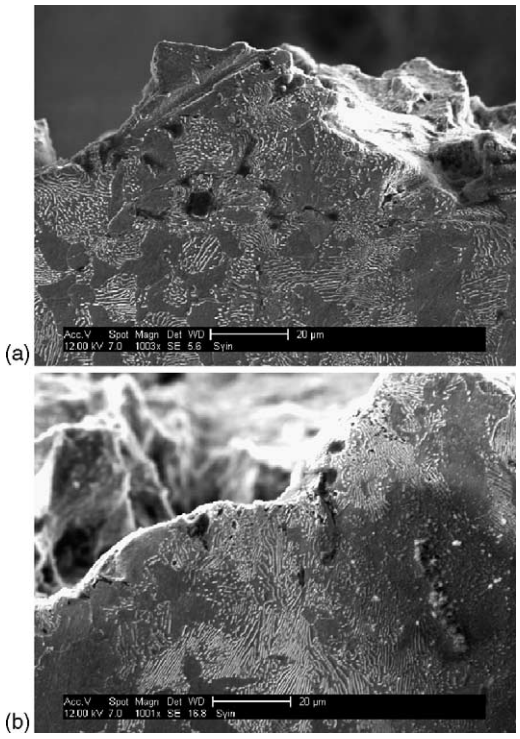

Fig. 3. SEM observation of microcracks in fracture surface layers: (a) microcracks in fracture surface layer caused by the Charpy impact test; (b) microcracks in fracture surface layer caused by slow bending test.

Mechanical properties of the surface layers right beneath the fracture surface were measured using a micro-mechanical probe. Results of the test are shown in Figs. 5 and 6, respectively. As illustrated in Fig. 5, slow-bending resulted in the highest hardness (HV 269) followed by the Charpy impact test (HV 254), and the annealed sample had the lowest (HV 147).

Fig. 6 illustrates the variations in micro-hardness as a function of the distance from the fracture surface. As shown, the affected layers are rather thick. The impact-fractured sample has a deformed layer of about 2800 μm while that of the slow bending-fractured sample is 4200 μm thick. The hardness of

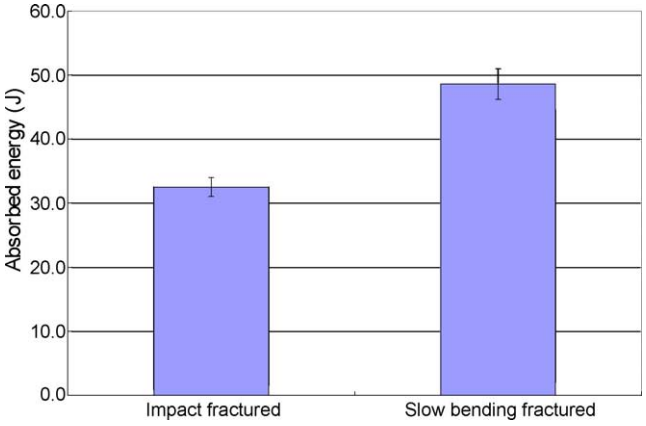

Fig. 4. Absorbed energies of Charpy impact and slow bending tests.

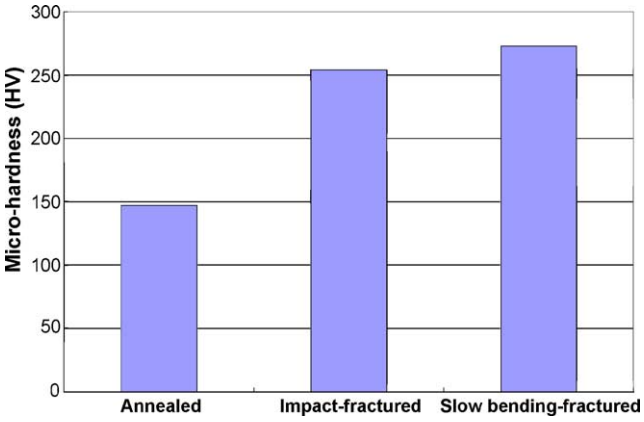

Fig. 5. Micro-hardness of annealed, impact-fractured and slow bending-fractured sample surface.

the very surface is lower than the sub-surface layer. This could be attributed to microcracks in the near surface layer, which could make the layer less resistant to indentation.

The X-ray diffractograms ((1 1 0) peak) of annealed, impact-fractured and slow bending-fractured samples are superimposed in Fig. 7. (2 2 0) peaks were also analysed. The X-ray line profile analysis results are summarized in Table 1. It is shown that the slow-bending yielded larger microstrain (0.0401%) than Charpy impact (0.0230%). In addition, the diffraction peaks of both slow bending-fractured and impact-fractured surface layers were found to shift to the left with respect to that of the annealed sample, which indicate the

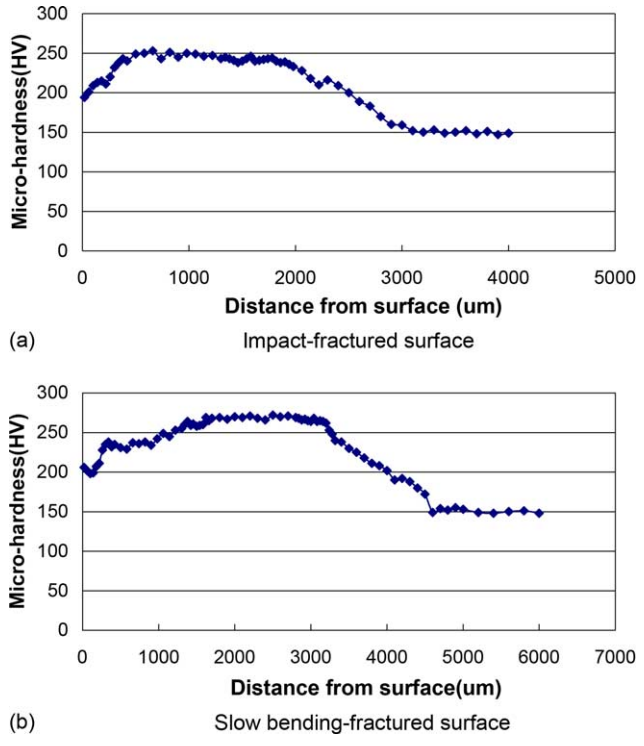

Fig. 6. Micro-hardness of impact-fractured and slow bending-fractured surface layers: (a) impact-fractured surface; (b) slow bending-fractured surface.

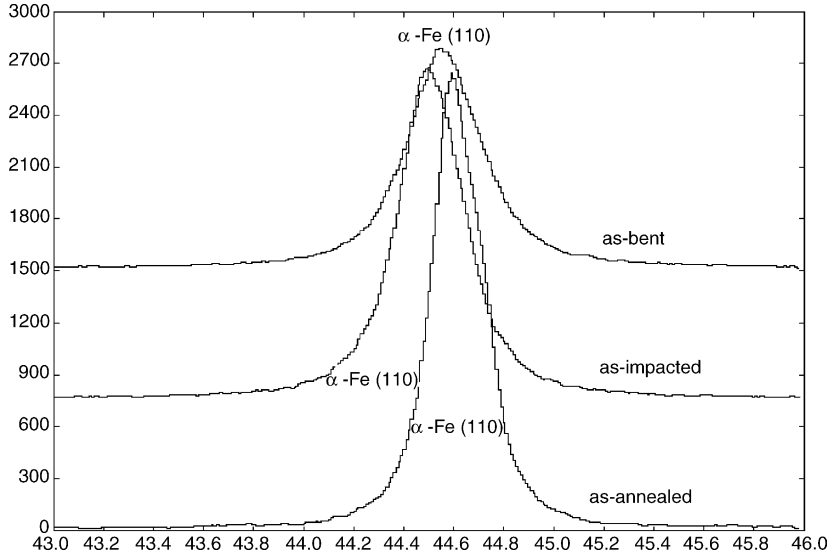

Fig. 7. X-ray (1 1 0) diffractions of full-annealed, impact-fractured and slow bending-fractured surface layers.

presence of residual tensile stress normal to the fracture surface [4].

One of our tasks is to investigate the surface microstructure and defect configuration resulting from different loading rates, mainly the dislocation density that strongly influences the electrochemical behaviour of materials. The XRD results indicate that the slow bending-fractured sample may have higher dislocation density than the impact-fractured sample, because its larger residual microstrain should mainly result from higher dislocation density. The XRD result is consistent with that of the micro-indentation test. For instance, the slow-bending sample had a higher microhardness than the impact-fractured sample. This could be mainly attributed to the strain-hardening effect that is dependent on the number of dislocations.

The higher dislocation density of the slow bending-fractured surface layer may also be expected based on the absorption energy measurement. The absorbed energies (E) during fracture can be basically resolved into two components: the plastic strain energy (W_d) and the surface energy (W_s) of the fracture surfaces as well as those of microcracks:

$$E = W_d + W_s \quad (1)$$

The fracture surface and cross-sectional SEM examinations have shown that the impact-fractured and slow bending-fractured surface have similar roughness. Although the former shows more microcracks, the difference in the crack density between the fracture surface layers are not large, at least on the same order of magnitude. Therefore, the higher absorbed energy of the slow bending-fractured sample may imply that it experienced larger plastic deformation than the impact-fractured one. A higher dislocation density is thus expected for the slow bending-fractured sample. However, it should be pointed out that the thicker plastic deformation layer of the slow bending sample also consumed part of the absorbed energy. Nevertheless, the dislocation density of the slow bending-fractured surface layer should be higher, not only supported by all the experimental results but also expected theoretically.

Table 1
Results of the X-ray line profile analysis

	Integral broadening (1 1 0)	Integral broadening (2 2 0)	Microstrain (%)
Impact-fractured	0.0016	0.0020	0.0230
Bending-fractured	0.0025	0.0032	0.0401

t

The differences in residual microstrain and dislocation density between slow bending-fractured and impact-fractured surface layers could be explained in terms of dislocation dynamics: the behaviour of dislocations moving at high speeds is quite different from that of quasi-static ones [7]. If we assume that a dislocation has an equivalent mass (m^*), the force (F) required to drive the dislocation with a certain acceleration (a) may be determined by Newton's law of motion [7]:

$$F = m^* a \quad (2)$$

Therefore, there must be a drag force to hold back the dislocation before a certain velocity is reached. The larger the acceleration, the larger the drag force. Thus, when a sample is deformed at a high strain rate, dislocations are relatively difficult to be generated and moved. As a result, the dislocation density would be possibly low and plastic deformation could be restricted to relatively small local regions. Less plastic deformation with lower dislocation density could therefore be expected in samples experienced the Charpy impact test, in which the strain rate at the notch tip was estimated to be in the range of 10^2–10^3 s^{-1} [8].

Thus, under the Charpy impact condition, brittle fracture was the main failure mode with less plastic deformation involved. The deformation caused by the impact force could be accommodated by microcracking. From this point of view, a relatively lower dislocation density can be expected for the impact-fractured sample.

The dynamic behaviour of materials, i.e. deformation at high strain rates has been a subject of numerous studies for recent decades, due to its significance to engineering practice [2,7]. Many investigators have examined the effects of strain rate on the dislocation substructure by means of transmission electron microscopy (TEM) [9–11]. In many cases, a cellular dislocation substructure develops, and the dislocation density increases with strain rate; while the dislocation cell size decreases with the strain rate. As a consequence, microhardness and flow stress have been found to increase with the strain rate. It seems that the results obtained in this study conflict with the previous studies reported in literature. However, it must be pointed out that the previously reported experimental results were obtained using the Split-Hopkinson-pressure-bar technique, in which a specimen was deformed under compressive stress. In a compressive stress state, the number of microcracks could be smaller than that under tensile stress, bearing in mind that compressive stress can not result in cracking. Therefore, more dislocations must be introduced to accommodate deformation under the applied stress. This could be a reason why under compressive stress at high strain rates, more dislocations could be generated but moved in local regions, thus resulting in small dislocation cells. However, in the Charpy impact test, the stress in the vicinity of notch tip is complicated but basically tensile in nature [12,13], which favours the formation of microcracks. Under such a condition, less plastic deformation was involved and cleavage fracture could thus be the main failure mode. All experimental observations in this study are consistent with the theoretical argument.

3.2. Corrosion behaviour

The Potentiodynamic polarization curves of the 1045 steel of different states measured in 3.5% NaCl solution at room temperature (~22 °C) are shown in Fig. 8. Table 2 summarizes electrochemical properties obtained using Tafel method and linear polarization method. One may see that the slow bending-fractured sample has the highest corrosion rate, followed by the impact-fractured sample, and the annealed sample has the lowest corrosion rate.

In general, corrosion is an electrochemical reaction in which a metal loses electrons and dissolves in the corrosive

Table 2
Results of the electrochemical test

	Ecorr (mV)	Icorr (μA/cm^2)	R_p (Ω/cm^2)
Annealed	−584 ± 7	6.93 ± 0.23	1266 ± 84
Impact-fractured	−668 ± 10	14.78 ± 0.53	1143 ± 77
Bending-fractured	−695 ± 12	19.19 ± 0.44	934 ± 85

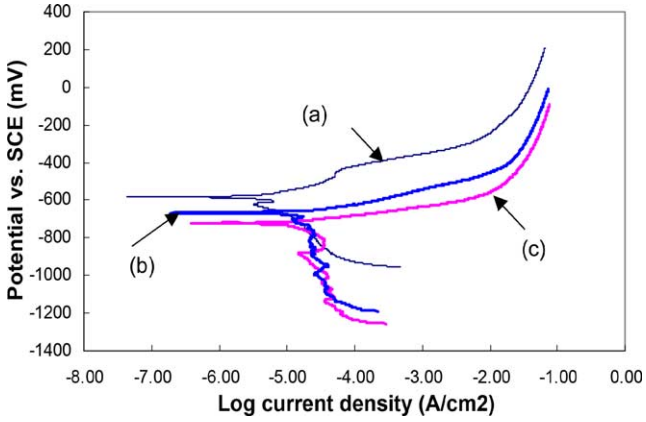

Fig. 8. Potentiodynamic polarization curves of different surfaces in 3.5% NaCl solution: (a) full annealed; (b) Charpy impact fractured; (c) slow bending-fractured.

solution. The activity of electrons may be reflected by the electron work function, the minimum energy required to remove electrons from inside a metal to its surface with zero kinetic energy [14]. In order to better understand the above electrochemical results, the electron work functions (EWF) of the three types of sample surface were measured using a scanning Kelvin probe. Results of the test are shown in Fig. 9. As shown, the slow bending-fractured surface has the lowest EWF (4.1–4.3 eV), followed by the impact-fractured surface (4.4–4.6 eV), and the annealed sample has the highest EWF (4.6–4.7 eV).

It has been demonstrated that the EWF decreases with plastic deformation no matter if it is tensile or compressive [15,16], which implies that dislocation renders electrons more active and thus increases the driving force for electrochemical reaction. This means that a deformed metal tends to lose electrons more easily than an unreformed one. Consequently, a heavily deformed metal should have a high corrosion rate, since its high-density dislocations provide a large number of active sites at which corrosion is promoted. Previous studies have demonstrated that the corrosion rate of a metal increases with an increase in the amount of plastic deformation [17]. The results of the electrochemical test in

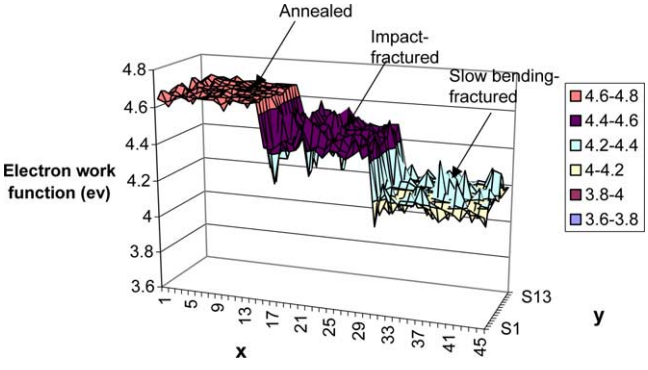

Fig. 9. Electron work functions of full-annealed, impact-fractured and slow bending-fractured surfaces.

this study are consistent with the EWF measurement and also expected based on our previous studies. In summary, since the slow bending-fractured surface layer has a higher dislocation density than the impact-fractured one, the former has a higher corrosion rate. Among the three types of samples, the annealed has the lowest corrosion rate. It should be mentioned that the EWF is also affected by surface roughness. However, since the impact-fractured surface and the slow bending-fractured one have similar roughness, the effect of roughness on EWFs of these two surfaces could be largely minimized or the roughness effect on the difference in EWF between these two surfaces could be negligible. As for the annealed sample, it should have higher EWF than the two fractured surfaces, because of its lower dislocation density or dislocation-free state.

3.3. Corrosive wear behaviour

The corrosive wear behaviour of the samples was evaluated using scratching test in 3.5% NaCl solution under different loads. After scratching, cross-sectional profiles of the scratch grooves were measured under an atomic force microscope (AFM). The wear rate is represented by the volume loss per unit length of the scratch groove (mm^3/mm). As an example, Fig. 10 illustrates the cross-sectional profiles of grooves scratched under a load of 5 g. The wear rate results are summarized in Fig. 11.

As illustrated, under different loads, the samples performed differently. At the low load of 5 g, the slow bending-fractured and impact-fractured sample have close wear rates that are lower than that of the annealed sample. When the applied load increased, the situation was reversed. At the load of 10 g, wear rates of the slow bending-fractured and impact-fractured samples are still close but higher than that of the annealed one. At the load of 30 g, the impact-fractured samples have a markedly higher wear rate than the slow bending-fractured samples.

The observed performances of the three types of samples can be explained. It is generally accepted that the wear loss is approximately inversely proportional to the hardness of the target material [18]. The slow bending-fractured and impact-fractured surfaces are harder than the annealed one, due to the strain-hardening effect that more or less benefited the wear resistance [17]. As a result, the slow bending-fractured and impact-fractured surfaces, although their toughness was lower, could show higher resistance to wear than the annealed one under low wear force. However, if the wearing force is large, the situation could be different. Under relatively higher loads, the fracture stress might be reached and all the samples would experience relatively severe wear. Under such a condition, the softer sample (annealed) might have improved performance relative to the strain-hardened ones, since it may have larger contact area and thus smaller contact stress, which may decrease the wear damage. In addition, the higher ductility of the annealed sample helps to accommodate deformation and this may reduce nucleation and propagation of cracks.

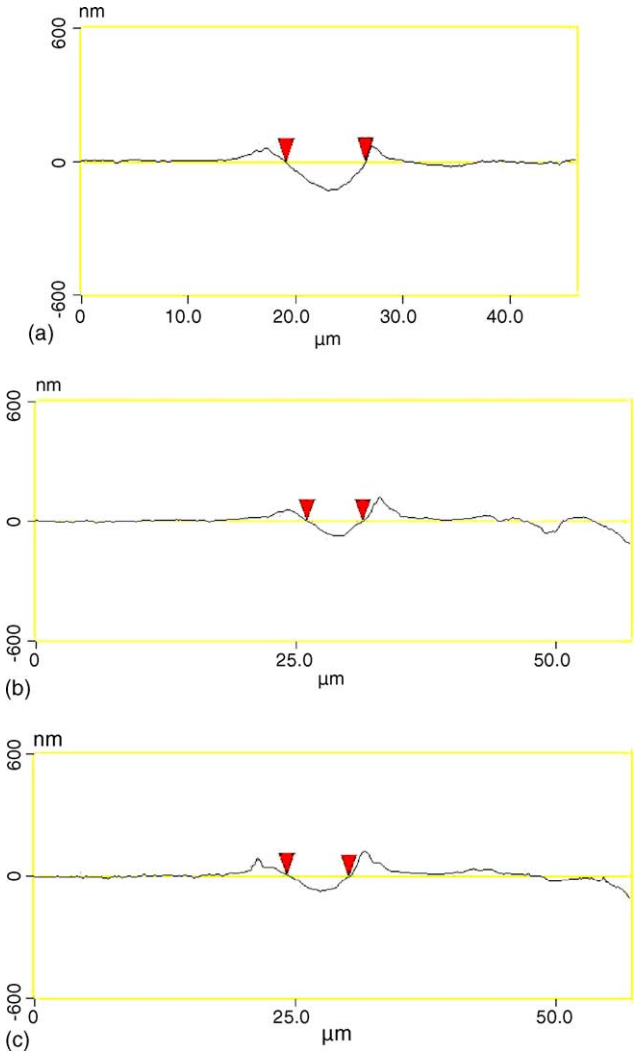

Fig. 10. Cross-sectional profiles of scratch grooves generated by scratch in 3.5% NaCl solution at a load of 5 g: (a) annealed; (b) impact-fractured; and (c) slow bending-fractured.

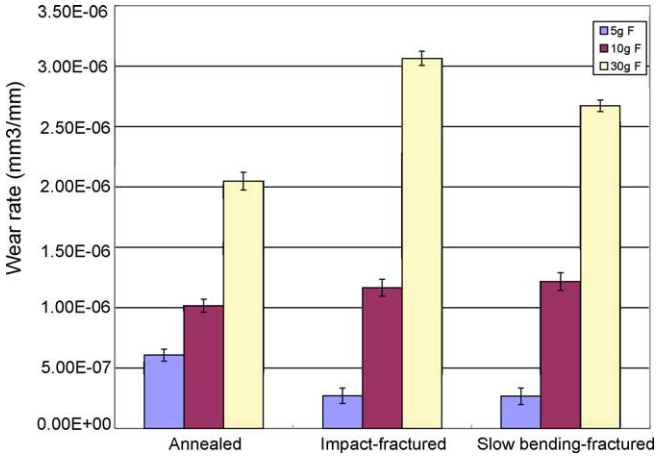

Fig. 11. Wear rates of annealed, impact-fractured, slow bending-fractured surfaces caused by scratch in the 3.5% NaCl solution.

It must be indicated that the larger volume loss of the fractured surfaces under the load of 30 g may be caused by the accelerating effect of corrosion on wear that can be enhanced by defects. The negative effect of defects, e.g., dislocations, on corrosion has been demonstrated by the electrochemical tests and EWF measurements in the present study. In addition, the microcracks and dislocations in the fractured surface layers led to a decrease in toughness, thus reducing the wear resistance under relatively larger wearing forces.

It is interesting to notice that, under the highest load of 30 g force, the Charpy impact-fractured sample showed slightly higher volume loss than the bending-fractured sample. This might be ascribed to the surface defect structure. For the impact-fractured surface layer, the dislocation density could be lower than that in the slow bending-fractured surface layer because of the high strain rate as discussed earlier. Instead, the density of microcracks beneath surface could be relatively higher than that of slow bending-fractured sample. The microcracks may act as stress raiser and made the surface vulnerable to wear attack especially under large wearing forces. When immersed in the corrosive solution, material degradation and stress-corrosion cracking at the crack tip could largely accelerate the surface wear failure, leading to a higher wear rate.

It should be mentioned that the surface deformed layers of the impact-fractured and slow bending-fractured samples had different thickness values (Fig. 6), which might influence the difference in wear behaviours between the fractured surfaces. However, the deformed layers were quite thick ($\sim 10^3$ μm). Under the scratch test condition, where the scratch depth was in the order of magnitude of 10–10^2 nm (Fig. 10), the difference in the depth of the deformed layers should therefore not be responsible for the difference in wear performance between the impact-fractured and slow bending-fractured surfaces.

4. Conclusions

Effects of the loading speed or strain rate on corrosion and corrosive wear of annealed, impact-fractured and slow bending-fractured surface layers of AISI 1045 steel in a 3.5% NaCl solution were investigated. The results showed that the slow bending-fractured surface layer had the highest dislocation density and hardness, followed by the impact-fractured one, and the annealed sample had the lowest dislocation density and hardness. The effect of the strain rate on the dislocation density could be explained based on the dislocation dynamics and fracture mode. Electrochemical tests demonstrated that the slow bending-fractured surface had the highest corrosion rates, followed by the impact-fractured one, and the annealed one had the lowest corrosion rate. Such difference in corrosion rate could be mainly attributed to different dislocation densities, which influence the surface electron activity. Using electrochemical scratching tests, the corrosive wear performances of the three groups of samples were evaluated. It was demonstrated that under a low load of 5 g, the slow bending fractured and impact-fractured surfaces had higher wear resistance than the annealed one, while under higher loads, the situation was reversed. Under the highest load of 30 g, the impact-fractured surface showed the lowest resistance to corrosive wear.

Acknowledgements

The authors are grateful for financial support from the Alberta Energy Research Institute (AERI/COURSE PROGRAM) and the Natural Science and Engineering Research Council of Canada (NSERC).

References

[1] S.W. Watson, F.J. Friedersdorf, B.W. Madsen, S.D. Cramer, Methods of measuring wear-corrosion synergism, Wear 181–183 (1995) 476.
[2] T.Z. Blazynski (Ed.), Materials at High Strain rates, Elsevier, New York, 1987, p. 243.
[3] R. Liu, D.Y. Li, A study of the mechanism for beneficial effects of yttrium additive in lubricant on corrosive wear and friction of metals, ASTM STP 1339 (2001) 549.
[4] H.P. Klug, L.E. Alexander, X-Ray Diffraction Procedures for Polycrystalline and Amorphous Materials, second ed., Wiley, New York, 1974.
[5] I.D. Baikie, P.J. Estrup, Low cost PC based scanning Kelvin probe, Rev. Sci. Instrum. 69 (1998) 3902.
[6] X.Y. Wang, D.Y. Li, Investigation of the synergism of wear and corrosion using an electrochemical scratch technique, Tribol. Lett. 11 (2001) 117.
[7] M.A. Meyers, Dynamic Behaviour of Materials, Wiley, New York, 1994.
[8] S. Xu, G. Shen, R. Bouchard, W.R. Tyson, Effect of excess energy during impact on Charpy absorbed energy, Materials Technology Laboratory Report MTL 2002-6(TR).
[9] W.S. Lee, H.F. Lam, The deformation behaviour and microstructure evolution of high-strength alloy steel at high rate of strain, J. Mater. Process. Technol. 57 (1996) 233–240.
[10] K.P. Staudhammer, L.E. Murr, The effect of prior deformation on the residual microstructure of explosively deformed stainless steels, Mater. Sci. Eng. 44 (1980) 97–113.
[11] C.Y. Chiem, J. Duffy, Strain rate history effects and observations of dislocation substructure in aluminum single crystals following dynamic deformation, Mater. Sci. Eng. 57 (1983) 233–247.
[12] Standard test methods for notched bar impact testing of metallic materialsd, ASTM E23-02, 2004.;
Annual Book ASTM Standard, vol. 03.02, Wear and Erosion, Metal Corrosion, ASTM, Philadelphia, PA, 2004, pp. 144–169.
[13] R.W. Hertzberg, Deformation and Fracture Mechanics of Engineering Materials, third ed., Wiley, New York, 1994.
[14] N.W. Ashcroft, N.D. Mermin, Solid State Physics, Holt, Rinehart, and Winston, New York, 1976.
[15] D.Y. Li, Kelvin probing technique: a promising method for determination of the yield strain of a solid under different types of stress, Phys. Stat. Sol. 191 (2002) 427–434.
[16] W. Li, D.Y. Li, Effects of dislocations on the electron work function of a metal surface, Mater. Sci. Technol. 18 (2002) 1057.
[17] S.B. Yin, D.Y. Li, Effects of prior cold work on corrosion and corrosive wear of pure copper in HNO3 and NaCl solutions, Mater. Sci. Eng. A, in press.
[18] I.M. Hutchings, Tribology: Friction and Wear of Engineering Materials, Edward Arnold, London, 1992.